Proceedings of ASME Turbo Expo 2017: Turbomachinery Technical Conference and Exposition
GT2017
June 26-30, 2017, Charlotte, NC, USA

GT2017-64821

THE EFFECT OF LEWIS NUMBER ON INSTANTANEOUS FLAMELET SPEED AND POSITION STATISTICS IN COUNTER-FLOW FLAMES WITH INCREASING TURBULENCE

Sean D. Salusbury
McGill University
Montreal, Quebec, Canada

Ehsan Abbasi-Atibeh
McGill University
Montreal, Quebec, Canada

Jeffrey M. Bergthorson*
McGill University
Montreal, Quebec, Canada

ABSTRACT

Differential diffusion effects in premixed combustion are studied in a counter-flow flame experiment for fuel-lean flames of three fuels with different Lewis numbers: methane, propane, and hydrogen. Previous studies of stretched laminar flames show that a maximum reference flame speed is observed for mixtures with $\mathrm{Le} \gtrsim 1$ *at lower flame-stretch values than at extinction, while the reference flame speed for* $\mathrm{Le} \ll 1$ *increases until extinction occurs when the flame is constrained by the stagnation point. In this work, counter-flow flame experiments are performed for these same mixtures, building upon the laminar results by using variable high-blockage turbulence-generating plates to generate turbulence intensities from the near-laminar* $u'/S_L^o = 1$ *to the maximum* u'/S_L^o *achievable for each mixture, on the order of* $u'/S_L^o = 10$*. Local, instantaneous reference flamelet speeds within the turbulent flame are extracted from high-speed PIV measurements. Instantaneous flame front positions are measured by Rayleigh scattering. The probability-density functions (PDFs) of instantaneous reference flamelet speeds for the* $\mathrm{Le} \gtrsim 1$ *mixtures illustrate that the flamelet speeds are increasing with increasing turbulence intensity. However, at the highest turbulence intensities measured in these experiments, the probability seems to drop off at a velocity that matches experimentally-measured maximum reference flame speeds in previous work. In contrast, in the* $\mathrm{Le} \ll 1$ *turbulent flames, the most-probable instantaneous reference flamelet speed increases with increasing turbulence intensity and can, significantly, exceed the maximum reference flame speed measured in counter-flow laminar flames at extinction, with the PDF remaining near symmetric for the highest turbulence intensities.*

These results are reinforced by instantaneous flame position measurements. Flame-front location PDFs show the most probable flame location is linked both to the bulk flow velocity and to the instantaneous velocity PDFs. Furthermore, hydrogen flame-location PDFs are recognizably skewed upstream as u'/S_L^o *increases, indicating a tendency for the* $\mathrm{Le} \ll 1$ *flame brush to propagate farther into the unburned reactants against a steepening average velocity gradient.*

Introduction

Hydrodynamic stretch and curvature are crucial phenomena in premixed combustion and have been studied in detail for laminar flames [1–3]. In a laminar stagnation flame, stretch limits the reaction zone thickness and, at a critical stretch rate, causes extinction for flames with Lewis numbers ($\mathrm{Le} = \alpha/D$) near unity, where α is the thermal diffusivity and D is the mass diffusivity of the deficient reactant. For a diffusionally-balanced mixture with $\mathrm{Le} = 1$, extinction occurs near a laminar Karlovitz number of unity, $\mathrm{Ka}_L = 1$, with $\mathrm{Ka}_L = K\delta_L/S_L^o$, where K is flame stretch rate, δ_L is laminar flame thickness, and S_L^o is unstretched laminar flame speed. Laminar Karlovitz number is the ratio of a mixture's characteristic chemical reaction time and its characteristic flow time. For cases in which thermal diffusivity dominates ($\mathrm{Le} > 1$), maximum flame temperature falls below adia-

*Address all correspondence to jeffrey.bergthorson@mcgill.ca

batic flame temperature and decreases with increasing stretch, reducing heat release rates and causing extinction at lower flame stretch and laminar Karlovitz number than for Le = 1 flames, i.e. $Ka_{L,ext} < 1$. When Le $\ll 1$, burning rates are enhanced by differential molecular diffusion into the reaction zone and stretched flame temperature and flame speed are greater than the adiabatic flame temperature and unstretched laminar flame speed of the bulk mixture. Extinction occurs in such cases at $Ka_{L,ext} > 1$, only when the flow conditions force the reaction zone against the stagnation surface and its thickness, and the associated residence time available for chemical reactions, is reduced by the imposed physical constraint. These effects are supported by a recent study [4], which investigated lean methane-air, propane-air, and hydrogen-air mixtures using detailed experiments and numerical simulations.

The differential-diffusion effects discussed above for stretched laminar flames must also affect the local instantaneous burning rates of premixed turbulent flamelets, and a number of studies have investigated the effect of differential diffusion in turbulent flames [5–13]. Many studies of stretch effects in turbulent flames, both theoretical and experimental, have been conducted [10, 14–18]. In [17], direct numerical simulations (DNS) at increasing turbulence intensity show that as turbulence increases, flames approach the behaviour of critically-stretched laminar flames (e.g., Fig. 5(a) in [17]). This compelling result will be investigated experimentally in this paper. Work by [18] further motivates this study with results indicating that curvature effects alone are insufficient to explain increasing burning rates with increasing turbulence. Instead, increasing local flamelet speed through stretch will be studied experimentally in this paper. Further studies have examined the impact of curvature on the level-set formulation in turbulent jet flames [19], flame surface density and curvature [20, 21], and turbulent burning velocity or bulk burning rate [10, 15, 19, 22, 23], and even local flamelet measurements [24–27]. While such studies provide great insight and a wealth of experimental results, time-averaged measurements do not necessarily yield information on the physics of propagation mechanisms at an instantaneous scale. Instead of such average values, measurements of local, instantaneous flamelet properties are needed to advance our understanding, as many researchers, such as Driscoll [28], have suggested.

The powerfully simple geometry of the counter-flow burner provides clear boundary conditions and a compact experimental zone that is ideal for performing detailed local measurements of stretched, premixed flames. Counter-flow burners have been used in many fundamental studies of turbulent flames [29–31] as well as more recent investigations of detailed flame properties [4, 32–36]. The present paper will measure instantaneous reference flame speed and flame position of flames from the near-laminar case, extending the work presented in [4], and at increasing turbulence intensity. The maximum turbulence intensity achieved for each mixture is dictated by its extinction limit.

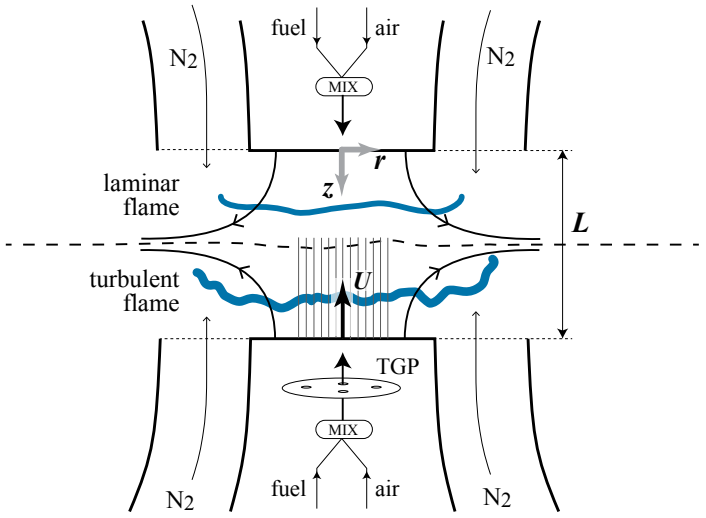

FIGURE 1. Schematic of turbulent and laminar flames in counter flow with location of bulk velocity, U, vertical lines indicating locations at which instantaneous velocity profiles are computed, turbulence generating plate (TGP) shown in lower turbulent nozzle, located upstream of the nozzle contraction 120 mm from the nozzle exit.

These mixtures represent low, unity, and high Lewis numbers in order to investigate the effects of differential diffusion in turbulent flame propagation.

Experimental method

Turbulent counter-flow burner

Experiments in this study are conducted using a counter-flow burner that consists of two identical nozzle assemblies arranged in vertical opposed flow. Premixed fuel and air jets are accelerated towards each other and meet at a stagnation surface. To extend the flammability limits of the lean turbulent flames in these experiments, the bottom nozzle delivers turbulent flow while the top nozzle delivers laminar flow, as illustrated in Fig. 1. The nozzle exits are separated by a distance of $L = 24$ mm, and the nozzle exit diameter is 20 mm.

Experiments in this paper will study hydrogen-air at $\phi = 0.19$, methane-air at $\phi = 0.6$, and propane-air at $\phi = 0.7$ under atmospheric pressure. The bulk flow velocity at the nozzle exit, U, varies between 0.5 m/s and 1.4 m/s in these experiments. These mixtures are selected to provide low, unity, and high Lewis numbers, respectively, while remaining stable in the counter-flow burner over a range of turbulence intensities. Properties of these mixtures are given in Table 1, with this study build-

ing upon the results for stretched laminar reference flame speeds for these same mixtures, reported recently [4].

Turbulence is generated by multi-circular jet high-blockage plates, following the work of [35, 37], which makes high turbulence intensity achievable in a compact, counter-flow apparatus. For multi-circular jet plates, turbulence intensity is a function of the radial position of the jet holes and their diameter, as well as the bulk flow velocity, U. These high-blockage plates have been shown to yield nearly isotropic turbulence statistics and high turbulence intensities [37], with values of $25\% \leq (u'/U) \leq 40\%$ typical in this study. Increasing turbulence is achieved in these experiments by increasing U and, thereby, increasing u', a consequence of which is the steepening of the average flow velocity gradient with increasing turbulence intensity.

Particle image velocimetry

For experiments in this study, high-speed PIV results are provided by a frame rate of 1000–3000 fps. The camera has a maximum resolution of 1024×1024 pixels at that frame rate and is used to capture an experimental region of approximately 30×30 mm, yielding a resolution of 34 pixels/mm. Flame intensity in PIV images is reduced with a bandpass filter at $\lambda = 527 \pm 10$ nm (Andover). Alumina particles of 1μm diameter are seeded into the flow and illuminated by a laser that emits 527 nm-wavelength light at 7.5 mJ per pulse. DaVis, a LaVision PIV software package, is used for two-dimensional PIV vector calculation. Typical particles occupy four pixels with eight to ten particles in each interrogation window.

In the calculation of mean turbulent statistics, 1000 PIV vector fields are averaged. Time between successive PIV vector fields, δt_{stat}, is kept greater than $\delta t_{\text{stat}} > 2 \times t_\Lambda$, where t_Λ is the integral time scale. This criterion ensures that each PIV vector field is statistically independent [38, 39]. The root-mean-square of the fluctuating component of velocity is referred to as the turbulence intensity, and is calculated from PIV data as:

$$u'(r,z) = \left(\frac{1}{T} \sum_{t=0}^{T} [u(r,z,t) - \langle u \rangle (r,z)]^2 \right)^{1/2} \quad (1)$$

where u is local instantaneous velocity, $\langle u \rangle$ is the local velocity averaged over time, r is the radial coördinate and z is the axial coördinate. The integral length scale, Λ, is calculated by spatial autocorrelation of PIV vector pairs. By this method, detailed in [40], Λ is determined by computing the integral of the autocorrelation function to the point at which it reaches a minimum. Experimental conditions of the runs reported in this paper are listed in Table 2, including bulk velocity at the nozzle outlet, $U = \langle u \rangle (r = 0, z = 24\,\text{mm})$, turbulence intensities u'/S_L^o, the estimates of Λ, and the turbulent combustion regime for each run

TABLE 1. Laminar flame properties for mixtures used in this study, with starred values measured in [4].

	CH_4+ Air $\phi = 0.6$	C_3H_8 + Air $\phi = 0.7$	H_2 + Air $\phi = 0.19$
Le	0.972	1.86	0.319
δ_L	0.450 mm	0.245 mm	0.580 mm
T_ad	1670 K	1860 K	897 K
S_L^o	11.5 cm/s	19.7 cm/s	8.75 cm/s
* $S_\text{u,max}$	24.6 cm/s	24.4 cm/s	31.4 cm/s
* $S_\text{u,max}/S_\text{L}^\text{o}$	2.14	1.24	3.59
* $\text{Ka}_\text{L,ext}$	1.39	0.354	3.00

based on the turbulent Karlovitz number, Ka_T, where

$$\text{Ka}_\text{T} = 0.157 \left(\frac{u'}{S_\text{L}^\text{o}} \right)^2 \text{Re}_\Lambda^{-0.5} \quad (2)$$

from [5], with the turbulent Reynolds number in the range of $18 \leq \text{Re}_\Lambda \leq 120$, with

$$\text{Re}_\Lambda = \frac{u'\Lambda}{\nu} \quad (3)$$

where ν is the kinematic viscosity.

Processed PIV images allow mean flow properties to be measured for each case. Sample flow measurements are shown for methane-air in Fig. 2. Axial velocity with respect to vertical location, z, is shown in Fig. 2(a) for three bulk flow rates, with $z = 0$ at the top nozzle and $z = 24$ mm at the exit of the bottom, turbulent nozzle (see Fig. 1). In Fig. 2(a), the mean velocities are seen to decrease towards the stagnation surface with little to no visible rise in velocity on the turbulent side as the process of averaging axial velocity acts to filter out this feature seen in steady laminar flames (see Fig. 3). The top-hat shape of the mean radial bulk-flow profile, with some curvature caused by the stagnation-flow pressure field, is shown in Fig. 2(b), measured at a location of $z = 22$ mm (above the turbulent nozzle). Finally, a contour plot of RMS fluctuations, u', is shown in Fig. 2(c), illustrating the steadiness of u' upstream of the mean flame location, as well as the value of turbulence intensity ahead of the flame, with respect to the bulk velocity at the outlet, is $u'/U \approx 40\%$. The area of asymmetric u' seen from $-10 \leq r \leq 0$ mm, centred at $z = 20$ mm, is an artifact resulting from interference in the PIV images due to scattered laser light off the rim of the brass nozzle.

Instantaneous axial velocity profiles are measured from processed PIV results at 1.0 mm radial intervals in the flame core, the region of the flame from $-5 \leq r \leq 5$ mm, as illustrated by

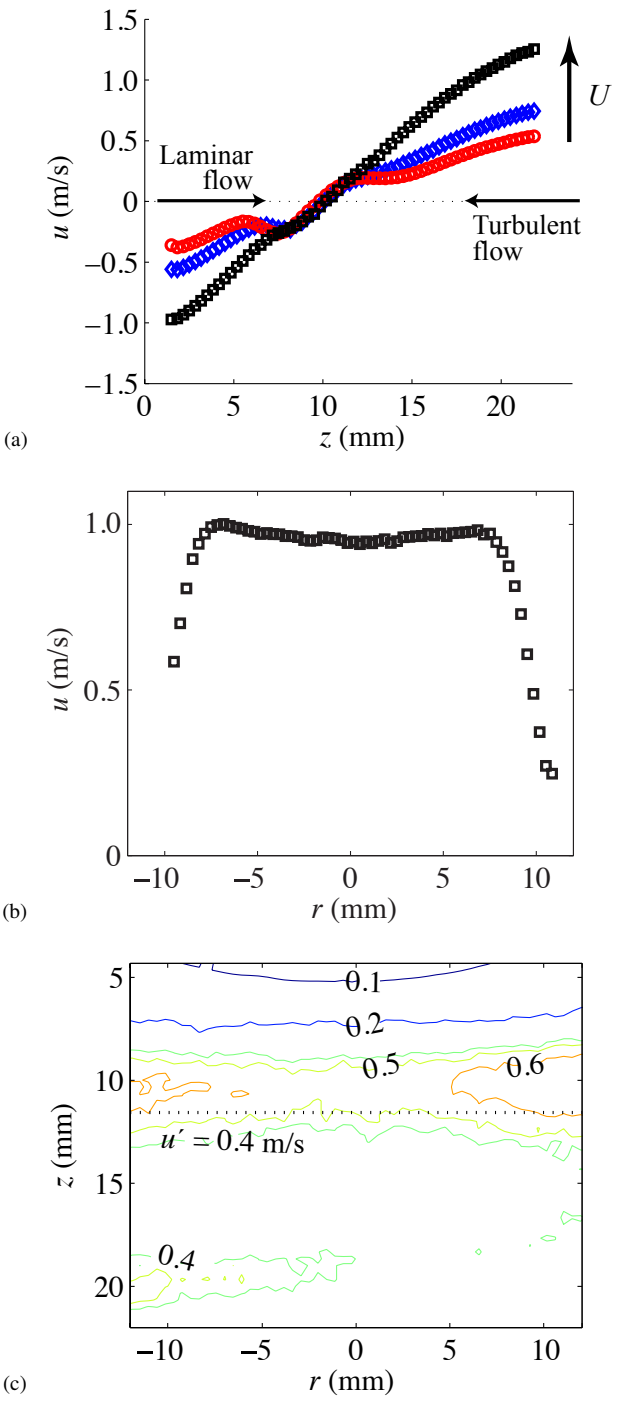

FIGURE 2. Flow profiles and contour plot of root-mean-square velocity for methane-air at $\phi = 0.6$: (a) axial profiles of axial velocity from PIV data for variable bulk flow rate, U, (b) radial profile of axial velocity measurements at $z = 22$ mm (above turbulent nozzle) for $U = 1.0$ m/s, (c) contour plot of velocity-fluctuation, u', measurements (solid lines) and mean flame brush location (dash line) for $u'/S_L^o = 2.3$ and $U = 1.0$ m/s.

TABLE 2. Experimental conditions of turbulent methane-air at $\phi = 0.6$ ($S_L^o = 11.5$ cm/s), propane-air at $\phi = 0.7$ ($S_L^o = 19.7$ cm/s) and hydrogen-air at $\phi = 0.19$ ($S_L^o = 8.75$ cm/s) experiments, indicating corrugated flame (C) and thin reaction-zone (TRZ) regimes. Experiments included in Figs. 5 – 7 shown in bold.

	U/S_L^o	u'/S_L^o	Λ/δ_L	Re_Λ	Ka_T	Regime
CH_4	**4.3**	**1.0**	**5.6**	**17.5**	**0.85**	**C**
	5.2	**1.5**	**5.8**	**26.6**	**1.3**	**TRZ**
	6.1	**2.3**	**5.6**	**40.7**	**2.0**	**TRZ**
	7.0	2.8	5.7	44.5	2.2	TRZ
	7.8	3.2	5.6	50.1	2.5	TRZ
	8.7	3.6	5.6	56.3	2.8	TRZ
	9.6	**4.6**	**5.6**	**78.7**	**3.8**	**TRZ**
	10.4	5.0	5.6	85.2	4.2	TRZ
	11.3	5.2	5.6	107.6	5.2	TRZ
C_3H_8	**2.5**	**1.0**	**9.8**	**33.3**	**1.6**	**TRZ**
	3.0	1.3	9.8	43.1	2.1	TRZ
	3.6	1.5	9.8	47.3	2.3	TRZ
	4.1	**1.6**	**9.7**	**60.1**	**3.0**	**TRZ**
	4.6	2.2	9.7	75.3	3.7	TRZ
	5.1	**2.9**	**9.9**	**104.4**	**5.1**	**TRZ**
	5.6	3.6	9.8	114.3	5.6	TRZ
	7.1	**3.8**	**9.9**	**119.8**	**5.9**	**TRZ**
H_2	5.7	1.0	4.6	17.5	0.92	C
	6.9	**1.6**	**4.5**	**20.9**	**1.1**	**TRZ**
	8.0	**2.5**	**4.6**	**33.6**	**1.8**	**TRZ**
	9.1	3.1	4.7	41.8	2.2	TRZ
	10.2	**4.1**	**4.6**	**52.6**	**3.0**	**TRZ**
	11.4	6.1	4.5	71.8	3.8	TRZ
	12.6	8.0	4.6	102.8	5.4	TRZ
	14.9	**10.5**	**4.6**	**118.3**	**7.6**	**TRZ**

the vertical lines in Fig. 1. Figure 3(b) shows instantaneous axial velocity profiles for the case of methane-air at $u'/S_L^o = 1.5$. The profiles in Fig. 3(b) show a local minimum in velocity that is not seen in the mean velocity profile in Fig. 2(a) due to the filtering effect that flame movement has on average velocity profiles. The velocity profiles of turbulent flamelets are seen to be similar to measurements of stretched laminar flames, shown at two flame stretch rates in Fig. 3(a). Local minima in the turbulent flame profiles, so-called reference flame speeds, $S_{u,ref}$, are identified and recorded by a MatLab script. The range of $S_{u,ref}$ values extracted from these profiles is indicated in Fig. 3(b). Since the local flame surface orientation is not computed at the point of local minimum, these values of $S_{u,ref}$ are assumed to be normal to the average flame surface. This assumption is true for

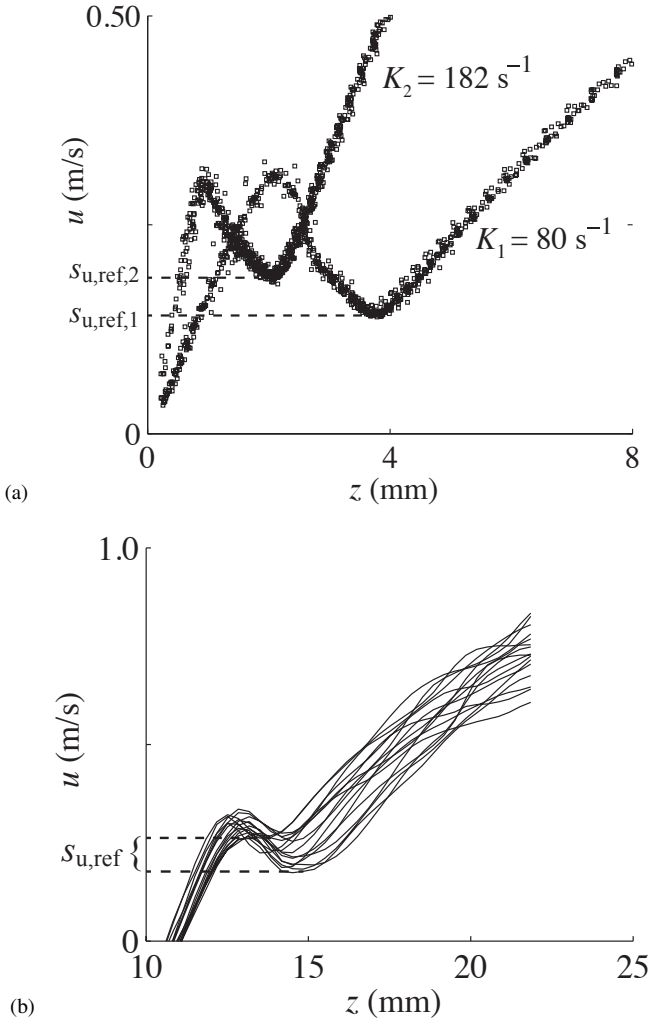

FIGURE 3. Velocimetry measurements of methane-air: (a) laminar velocity profiles at increasing stretch rate, with stagnation surface at $z = 0$, (b) instantaneous turbulent flamelet velocity profiles for methane-air at $u'/S_L^o = 1.5$. Flow is from right to left in both cases.

laminar flames for which the stationary flame surface is exactly perpendicular to the flow direction. Weakly turbulent flames diverge slightly from the laminar case with moderate curvature. For high-curvature cases, then, the perpendicularity assumption under-estimates $S_{u,ref}$ since the projection of the velocity vector in the axial direction is necessarily smaller than the vector itself. When considering the high-turbulence results in Figs. 5-7(a), it should, therefore, be noted that true $S_{u,ref}$ values may be higher than reported. However, resulting trends are unaffected.

Rayleigh scattering

Flame front location, flame curvature, and temperature progress variable for turbulent combustion experiments can be measured by planar Rayleigh scattering. Note that PIV and Rayleigh scattering measurements in this study are not simultaneous, since light scattered off the alumina particles during PIV would interfere with Rayleigh measurements. In these measurements, an ultra-violet light at $\lambda = 355\,\mathrm{nm}$ is used, which is collected by an iCCD camera.

The intensity of Rayleigh scattering is directly proportional to the number density of the gas, N. Number density can then be related to temperature directly by:

$$N = \frac{P}{kT} \tag{4}$$

where both Boltzmann's constant, k, and pressure, P, remain constant. As in [41], Rayleigh intensity is approximately related to temperature by:

$$T_{\mathrm{flame}} = \sigma\, T_{\mathrm{air}}\, \frac{I_{\mathrm{air}} - I_{\mathrm{back}}}{I_{\mathrm{flame}} - I_{\mathrm{back}}} \tag{5}$$

where T is temperature, σ is Rayleigh scattering cross-section of the stoichiometric fuel-air mixture with respect to the cross-section of standard air [42], and I is intensity counts: I_{air} is intensity in cold-flow images, I_{flame} is intensity in flame images, and I_{back} is background noise intensity. The average iCCD readout noise is equal to 86 counts and varies minimally. While it is possible to minimize ambient light and light scattered off optics, the reflections off components within the test section are difficult to eliminate. As a result, I_{back} is calculated by setting T_{flame} just downstream of the flame equal to the adiabatic flame temperature, T_{ad}, and solving Eqn. (5) for I_{back}, as in [43, 44]. This method preserves flame contour information across the images. Figure 4(a) show a sample Rayleigh image for a hydrogen-air flame and Fig. 4(b) shows the corresponding processed single-shot image.

Individual flame images are, then, thresholded and the Pavlidis contour tracing algorithm [45] is used to extract the flame surface location, z_f, for a progress variable of $c = 0.3$, as shown in Fig. 4(c), where c is defined as:

$$c = \frac{T - T_u}{T_{ad} - T_u}\,. \tag{6}$$

where $T_u = T_{air}$ in these experiments. Absolute flame position is sensitive to the choice of progress variable, but analysis in this paper will focus on relative flame position as turbulence intensity and Lewis number are varied. Measuring flame position at

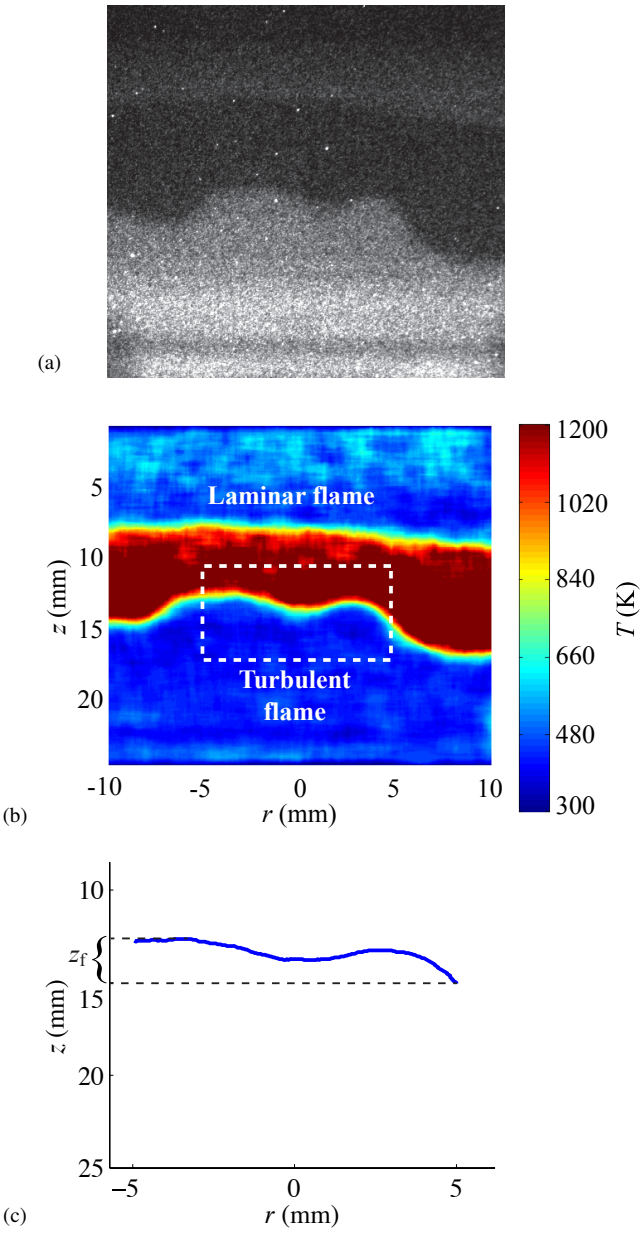

FIGURE 4. Single-shot Rayleigh images of hydrogen-air flame with $T_{ad} = 1180\,\mathrm{K}$ and turbulence intensity $u'/S_L^o = 2.5$: (a) raw image, (b) processed image, (c) turbulent flame contour with range of instantaneous flame locations, z_f, for region shown by dashed box in (b).

a higher or lower c value would simply translate resulting flame position distributions together, without noticeable change relative to one another (see Figs. 5-7(b)).

Laminar flames

The reference unburned flame speed, $S_{u,ref}$, of a laminar flame in stagnation flow is the minimum fluid velocity upstream of the flame surface, as illustrated in Fig. 3(a). The hydrodynamics of the laminar flame in stagnation flow is discussed thoroughly by Law [1] and in detail for this experimental geometry by Bergthorson *et al*. [46].

Experiments in stretched laminar flames have confirmed that $S_{u,ref}$ increases to a maximum at stretch rates below K_{ext} for near-unity Lewis number and $\mathrm{Le} > 1$ mixtures [4]. For mixtures with $\mathrm{Le} \ll 1$, reaction rates increase with stretch, increasing $S_{u,ref}$, and extinction only occurs because of the reduced residence time resulting from the flame being constrained by the stagnation surface at high stretch and bulk flow rates.

Table 1 summarizes the results from a previous study of stretched laminar methane, propane, and hydrogen flames [4], as well as laminar flame speed and thickness, δ_L, adiabatic flame temperature, T_{ad}, and computed Lewis numbers of these mixtures. Values of laminar Karlovitz number at extinctions, $\mathrm{Ka}_{L,ext}$, scale with Lewis number as discussed earlier. These stretched laminar flame results underscore the effects of differential diffusion and provide quantitative measures of the maximum stretched flame speeds that are the basis for the present investigation into premixed turbulent counter-flow flames.

Results and discussion

Maximum stretched laminar flame speed was shown to depend on the thermo-diffusive characteristics of the mixture; differential diffusion is now investigated in turbulent flamelets using PIV and Rayleigh scattering. Premixed turbulent flames of lean methane-air, propane-air, and hydrogen-air are studied at increasing u'/S_L^o, from the near-laminar case of $u'/S_L^o \approx 1$ to the maximum turbulence case for each fuel (see Table 2). In the current experimental configuration, for higher turbulence intensities and higher bulk flow velocities, the turbulent flames cannot be stabilized for long enough to allow the laser diagnostics to acquire meaningful statistics.

Instantaneous velocity profiles are extracted from PIV images (see Fig. 3(b)), and instantaneous $S_{u,ref}$ values are measured from these profiles. Instantaneous $S_{u,ref}$ values are compiled into a histogram that, for large sample sizes, approaches the probability density function (PDF) of reference flamelet speeds. For each PDF, approximately 8000 $S_{u,ref}$ values are included from instantaneous PIV vector fields. Instantaneous flame front position is also measured, using Rayleigh scattering, to build a PDF of instantaneous flame location taken from approximately 50 flame contour points in each of 500 total images.

Selected instantaneous reference flame speed PDFs and instantaneous flame position PDFs at variable turbulence intensity are shown side-by-side for the three Lewis-number cases in this study. Taken together, these PDFs are rich in physical informa-

tion about each mixture. For methane-air, Figs. 5(a) and 5(b) each contain four PDFs for increasing values of u'/S_L^o. First, in Figure 5(a), the unstretched laminar flame speed of the mixture and $S_{u,max}$, as measured in [4] and provided in Table 1, are both indicated in the figure. The key features of the PDFs in Fig. 5(a) are the shapes of the distributions and their most likely $S_{u,ref}$. The low turbulence case of $u'/S_L^o = 1.0$ shows a narrow PDF that is normally-distributed about the unstretched laminar flame speed. The flame at a low-turbulence case, therefore, approaches the behavior of a laminar methane-air flame; the overall increase in turbulent burning rate is primarily due to the increase in flame surface area, as proposed by Damköhler [47] and consistent with the understanding of flames in the corrugated flamelet regime.

As turbulence intensity increases, the width of the PDF and the most probable $S_{u,ref}$ both increase. At the highest u'/S_L^o case measured in these experiments, the most likely $S_{u,ref}$ is near $S_{u,max}$ and it seems that the probability drops off past $S_{u,max}$. However, more experimental data of instantaneous reference flamelet speeds is required at this higher range of u'/S_L^o to completely support this behavior.

Flame front position results for methane-air at increasing turbulence intensity are collected in Fig. 5(b) and show near-normal distributions, indicating that the flame brush neither has a tendency to burn downstream nor upstream towards unburned reactants. These results also show that the most probable location of the methane-air flame brush travels downstream as bulk velocity, U, and turbulence intensity, u', both increase, moving from $\langle z_f \rangle = 12\,\text{mm}$ at $U = 0.5\,\text{m/s}$ and $u'/S_L^o = 1.0$ to $\langle z_f \rangle = 10\,\text{mm}$ at $U = 1.3\,\text{m/s}$ and $u'/S_L^o = 4.6$. The flame moves only 2 mm as bulk velocity increases, indicating that flamelet speeds must increase substantially with increasing turbulence intensity. This allows the flame to stabilize in a zone of higher local velocity due to the steepening velocity profile with increasing U and u'/S_L^o (see Fig. 2(a)), a result that supports the findings of instantaneous velocity measurements from Fig. 5(a).

Probability distributions of $S_{u,ref}$ for propane at $\phi = 0.7$, a high-Lewis-number mixture, are shown in Fig. 6(a). Propane at $u'/S_L^o = 1.0$ shows a distribution peak near S_L^o and is comparatively narrow, approaching the laminar flame behaviour, as seen for methane at low turbulence intensity. Further results in Fig. 6(a) show that $S_{u,ref}$ distributions for moderate and high u'/S_L^o cases are wider. Unlike methane, in the case of propane, a peak in the high u'/S_L^o PDF is difficult to distinguish since that mixture's $S_{u,max}$ is close to its S_L^o.

Propane-air flame position statistics are shown together in Fig. 6(b). For propane, the width of the PDF, or flame brush, increases as u'/S_L^o increases, meaning that the flame front has a wider range of movement at higher u'/S_L^o. More noticeably, these results show that the most probable flame location moves significantly downstream with increasing bulk velocity and u'/S_L^o – from $\langle z_f \rangle = 17\,\text{mm}$ at $U = 0.6\,\text{m/s}$ and $u'/S_L^o = 1.0$ to $\langle z_f \rangle = 11\,\text{mm}$ at $U = 1.4\,\text{m/s}$ and $u'/S_L^o = 4.5$. Again, this behaviour is reinforced by instantaneous velocity measurements: most probable flamelet velocity increases only from $S_{u,ref} = 22.0\,\text{cm/s}$ to $S_{u,ref} = 24.4\,\text{cm/s}$, therefore, flame location must adjust more substantially in order to accommodate the increasing bulk velocity.

Results for the low-Lewis-number case of hydrogen and air at $\phi = 0.19$ are shown in Fig. 7(a). Differential-diffusion effects can be seen immediately in this figure. At the lowest u'/S_L^o measured, the most probable $S_{u,ref}$ is already seen to be approximately double S_L^o for hydrogen-air. The most probable $S_{u,ref}$ in Fig. 7(a) is seen to increase with u'/S_L^o with no apparent 'attracting' $S_{u,max}$. This result is explained by the impact of differential diffusion on low-Lewis-number mixtures: flame speed increases with positive stretch and curvature for lean hydrogen-air laminar flames and extinction is only brought on by imposing a bulk flow rate that physically forces the reaction zone against the stagnation plane. It is this constraint that reduces the residence time available for chemical reactions to occur and causes extinction in a laminar counter-flow flame [4]. In the turbulent case, the leading edges are not constrained and act to increase the flame burning rate by travelling up the velocity gradient into fresh reactants (see Fig. 2(a)).

The most probable flame location of hydrogen and air supports this argument: Fig. 7(b) shows that flame position remains at $\langle z_f \rangle \cong 8\,\text{mm}$, as bulk velocity increases from $U = 0.5\,\text{m/s}$ to $1.3\,\text{m/s}$ and turbulence intensity increases from $u'/S_L^o = 1.4$ to 10.5. Instantaneous flame speed is shown to increase significantly with u'/S_L^o, which compensates for the steepening velocity gradient and keeps the average flame position relatively constant. Hydrogen-air PDFs also show a result that is not as pronounced in methane or propane flames: there is a tail towards the turbulent cold flow in the hydrogen position distribution that extends as u'/S_L^o increases. In the flame location PDF, skewness represents the flamelets' preference for either burning upstream or downstream. An upstream tail, as seen for the hydrogen-air PDF in Fig. 7(b), is evidence of the leading flamelets making more frequent incursions into unburned reactants.

These experimental measurements of instantaneous velocity are consistent with the numerical work presented in [17]. Through analysis of DNS results of lean hydrogen-air flames with $\text{Le} \ll 1$, work in [17] shows that the mean flamelet velocity at the leading edges of highly turbulent flames approaches the behaviour of critically-stretched laminar flames. The observed instantaneous flamelet velocity PDFs presented in Fig. 7(a) for similar hydrogen-air flame experiments are consistent with the DNS results. In both cases, the most probable flamelet velocity increases with increasing turbulence intensity.

Figure 8 shows a summary of statistics extracted from the PDFs presented in this paper. In Fig. 8(a), the most probable reference flame speed, $\langle S_{u,ref} \rangle$, increases with turbulence intensity but plateaus near the maximum stretched laminar flame speed, $S_{u,max}$, for $\text{Le} \gtrsim 1$ mixtures and overshoots $S_{u,max}$ for the $\text{Le} \ll 1$

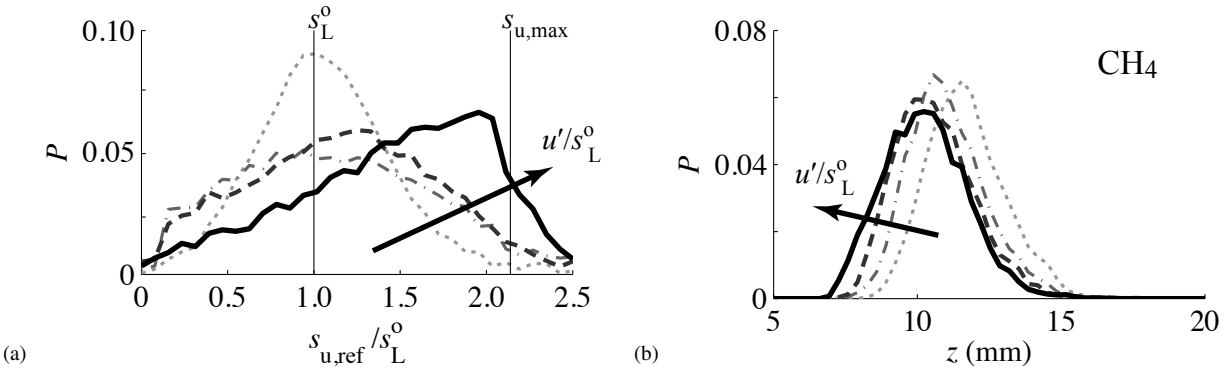

FIGURE 5. Instantaneous (a) $S_{u,ref}$ and (b) flame position of methane-air: $u'/S^o_L = 1.0$ (dot), $u'/S^o_L = 1.5$ (dash-dot), $u'/S^o_L = 2.3$ (dash), $u'/S^o_L = 4.6$ (solid).

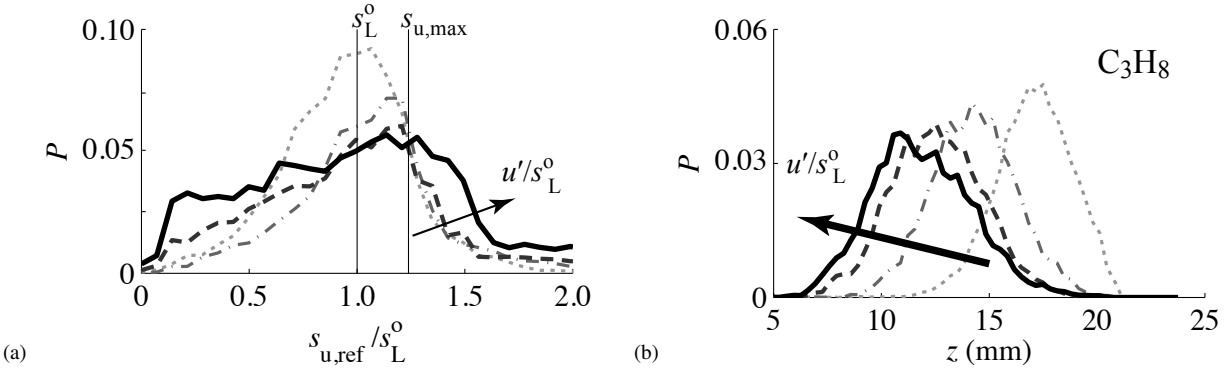

FIGURE 6. Instantaneous (a) $S_{u,ref}$ and (b) flame position of propane-air: $u'/S^o_L = 1.0$ (dot), $u'/S^o_L = 1.6$ (dash-dot), $u'/S^o_L = 2.9$ (dash), $u'/S^o_L = 3.8$ (solid).

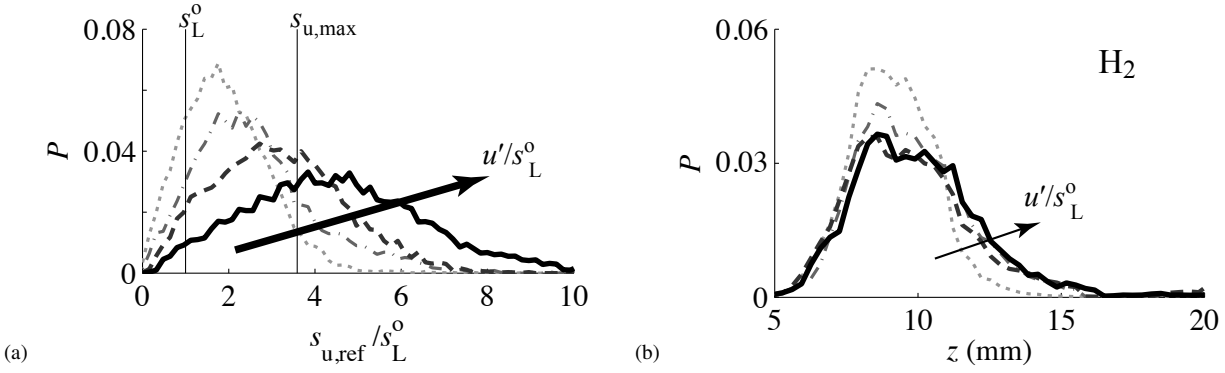

FIGURE 7. Instantaneous (a) $S_{u,ref}$ and (b) flame position of hydrogen-air: $u'/S^o_L = 1.6$ (dot), $u'/S^o_L = 2.5$ (dash-dot), $u'/S^o_L = 4.1$ (dash), $u'/S^o_L = 10.5$ (solid).

hydrogen-air mixture. Figure 8(b) shows that flames with Le $\gtrsim 1$ move downstream with increasing U and u'/S^o_L, while flames of lean hydrogen-air, with Le $\ll 1$, climb upstream. Figure 8(c) shows the average flow velocity at the most probable flame location, $\langle u \rangle(\langle z_f \rangle)$, averaged over the radial extent $-5 \leq r \leq 5$ mm. The average velocity at the most probable flame location is one possible definition of the turbulent burning velocity in a stagnation flow geometry [29]. Comparison of Figs. 8(a) and 8(c) shows that the instantaneous flamelet velocity statistics are directly reflected in the average turbulent flame speed, with very

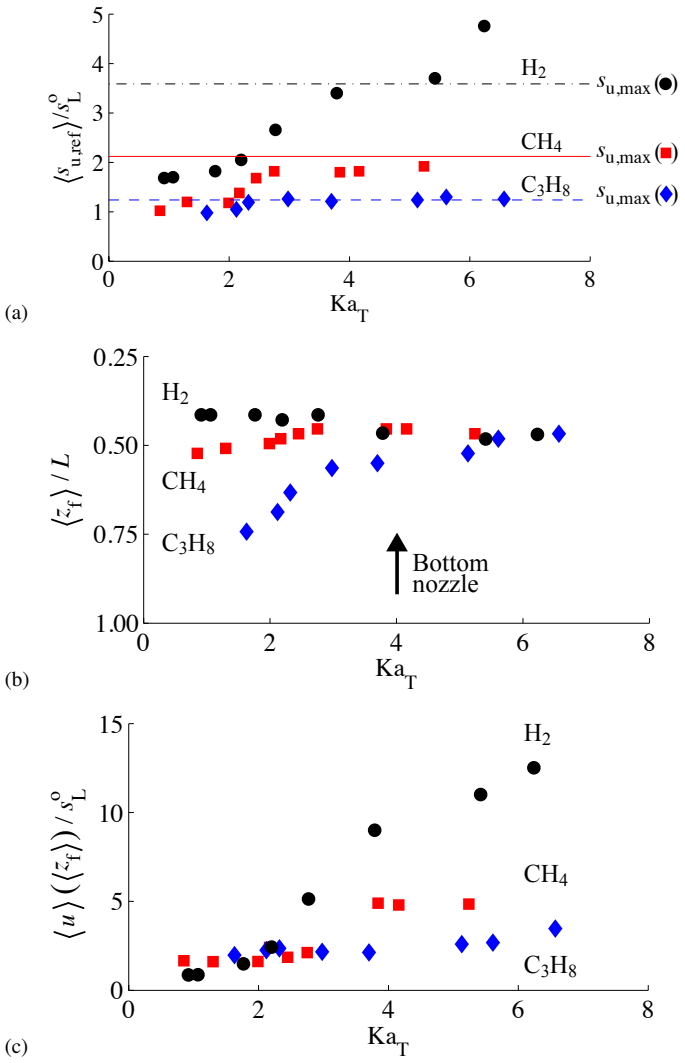

FIGURE 8. Summary plots of (a) most probable reference flame speed and maximum reference flame speed from [4] for propane (dash), methane (solid) and hydrogen (dash-dot), (b) most probable flame location and (c) average velocity, $\langle u \rangle (\langle z_f \rangle)$: methane-air with $\phi = 0.6$ (■), propane-air with $\phi = 0.7$ (♦), hydrogen-air with $\phi = 0.19$ (●).

different response of $\langle u \rangle (\langle z_f \rangle)$ to increasing $\mathrm{Ka_T}$ seen for fuels of different diffusivities. To increase turbulence intensity in these experiments bulk velocity is increased, which subjects the turbulent flames to a steeper average velocity gradients (see Fig. 2(a)). Mixtures with unity and high Lewis number are pushed further downstream by these gradients and their turbulent flame speeds increase only modestly with increasing u'. Conversely, low-Lewis number hydrogen can climb upstream to an average flame position at a higher average velocity, allowing its turbulent flame speed to increase substantially with increasing turbulence intensity. These results are echoes of the instantaneous flame speed results.

Conclusions

The effect of fuel diffusivity on propagation characteristics of premixed, turbulent flames was studied in a counter-flow experimental apparatus, from near-laminar flames to near-extinction conditions. Particle image velocimetry was used to measure the velocity field and turbulence intensity of the flow, and the instantaneous reference flamelet speeds in low, unity, and high Lewis-number mixtures. Instantaneous flame position was measured for these mixtures using Rayleigh scattering. Results of these measurements lead to the following conclusions:

1. Instantaneous reference flame speed measurements show that, in the case of $\mathrm{Le} \geq 1$ mixtures, flame speed is increasing with increasing turbulence. However, the flamelets tendency to a maximum $S_{u,ref}$ is not quite obvious from these experiments. It seems that more experimental data of instantaneous reference flamelet speeds, covering higher range of u'/S^o_L, is required to completely support the idea that $S_{u,max}$ is a limiting velocity for $\mathrm{Le} \geq 1$ mixtures.
2. Instantaneous reference flame speed of $\mathrm{Le} \ll 1$ flamelets increases with increasing u'/S^o_L without any limit found in these experiments. This result shows that there is no thermo-diffusive limiting $S_{u,max}$ for $\mathrm{Le} \ll 1$ mixtures within this range of turbulence intensities.
3. The position of methane-air and propane-air flames shifts downstream with increasing bulk flow since flamelet velocities cannot increase enough with increasing u'/S^o_L - due to the limiting effects of differential diffusion - to counteract the increasing bulk flow rate and velocity gradient.
4. Lean hydrogen-air, with $\mathrm{Le} \ll 1$, produces non-equidiffusive flames whose flame location distributions indicate a propensity for the flamelet to burn upstream into fresh reactants against the steepening average velocity gradient.
5. The instantaneous flamelet speed and position statistics demonstrate similar trends to the observed average burning rate of the turbulent flames. Flamelets that burn faster and propagate upstream lead to higher turbulent flame speeds.

ACKNOWLEDGMENT

This research was funded by the Natural Sciences and Engineering Research Council of Canada and Siemens Canada under the Collaborative Research and Development program (NSERC-CRD).

REFERENCES

[1] Law, C., 1988. "Dynamics of stretched flames". *Proceedings of the Combustion Institute,* ***22***, pp. 1381–1402.

[2] Williams, F. A., 2000. "Progress in knowledge of flamelet structure and extinction". *Progress in Energy and Combustion Science,* ***26***, pp. 657–682.

[3] Pitz, R. W., Hu, S., and Wang, P., 2014. "Tubular premixed and diffusion flames: Effect of stretch and curvature". *Progress in Energy and Combustion Science,* ***42***, pp. 1–34.

[4] Salusbury, S. D., and Bergthorson, J. M., 2015. "Maximum stretched flame speeds of laminar premixed counter-flow flames at variable Lewis number". *Combustion and Flame,* ***162***, pp. 3324–3332.

[5] Abdel-Gayed, R., Bradley, D., Hamid, M., and Lawes, M., 1984. "Lewis number effects on turbulent burning velocity". *Proceedings of the Combustion Institute,* ***20***, pp. 505–512.

[6] Lipatnikov, A., and Chomiak, J., 2005. "Molecular transport effects on turbulent flame propagation and structure". *Progress in Energy and Combustion Science,* ***31***, pp. 1–73.

[7] Venkateswaran, P., Marshall, A., Shin, D. H., Noble, D., Seitzman, J., and Lieuwen, T., 2011. "Measurements and analysis of turbulent consumption speeds of H2/CO mixtures". *Combustion and Flame,* ***158***, pp. 1602–1614.

[8] Barlow, R. S., Dunn, M. J., Sweeney, M. S., and Hochgreb, S., 2012. "Effects of preferential transport in turbulent bluff-body-stabilized lean premixed CH4/air flames". *Combustion and Flame,* ***159***, pp. 2563–2575.

[9] Regele, J. D., Knudsen, E., Pitsch, H., and Blanquart, G., 2013. "A two-equation model for non-unity lewis number differential diffusion in lean premixed laminar flames". *Combustion and Flame,* ***160***, pp. 240–250.

[10] Venkateswaran, P., Marshall, A., Seitzman, J., and Lieuwen, T., 2013. "Pressure and fuel effects on turbulent consumption speeds of H2/CO blends". *Proceedings of the Combustion Institute,* ***34***, pp. 1527–1535.

[11] Lin, Y.-C., Jansohn, P., and Boulouchos, K., 2014. "Turbulent flame speed for hydrogen-righ fuel gases at gas turbine relevent conditions". *International Journal of Hydrogen Energy,* ***39***, pp. 20242–20254.

[12] Savard, B., and Blanquart, G., 2014. "An a priori model for the effective species Lewis numbers in premixed turbulent flames". *Combustion and Flame,* ***161***, pp. 1547–1557.

[13] Savard, B., Bobbitt, B., and Blanquart, G., 2015. "Structure of a high Karlovitz n-C7H16 premixed turbulent flame". *Proceedings of the Combustion Institute,* ***35***, pp. 1377–1384.

[14] Libby, P. A., and Williams, F. A., 1982. "Structure of laminar flamelets in premixed turbulent flames". *Combustion and Flame,* ***44***, pp. 287–303.

[15] Chen, Y.-C., and Bilger, R. W., 2004. "Experimental investigation of three-dimensional flame-front structure in premixed turbulent combustion: II. Lean hydrogen/air bunsen flames". *Combustion and Flame,* ***138***, pp. 155–174.

[16] Dinkelacker, F., Manickam, B., and Muppala, S., 2011. "Modelling and simulation of lean premixed turbulent methane/hydrogen/air flames with an effective Lewis number approach". *Combustion and Flame,* ***158***, pp. 1742–1749.

[17] Amato, A., Day, M., Cheng, R., Bell, J., and Lieuwen, T., 2015. "Leading edge statistics of turbulent, lean, H2–air flames". *Proceedings of the Combustion Institute,* ***35***, pp. 1313–1320.

[18] Marshall, A., Lundrigan, J., Venkateswaran, P., Seitzman, J., and Lieuwen, T., 2015. "Fuel effects on leading point curvature statistics of high hydrogen content fuels". *Proceedings of the Combustion Institute,* ***35***, pp. 1417–1424.

[19] Yuen, F., and Gülder, O., 2009. "Premixed turbulent flame front structure investigation by Rayleigh scattering in the thin reaction zone regime". *Proceedings of the Combustion Institute,* ***32***, pp. 1747–1754.

[20] Gülder, O., and Smallwood, G., 2007. "Flame surface densities in premixed combustion at medium to high turbulence intensities". *Combustion Science and Technology,* ***179***, pp. 191–206.

[21] Yuen, F., and Gülder, O., 2010. "Dynamics of lean-premixed turbulent combustion at high turbulence intensities". *Combustion Science and Technology,* ***182***, pp. 544–558.

[22] Kobayashi, H., Tamura, T., Maruta, K., Niioka, T., and Williams, F. A., 1996. "Burning velocity of turbulent premixed flames in a high-pressure environment". *Proceedings of the Combustion Institute,* ***26***, pp. 389–396.

[23] Yamamoto, K., Ozeki, M., Hayashi, N., and Yamashita, H., 2009. "Burning velocity and OH concentration in premixed combustion". *Proceedings of the Combustion Institute,* ***32***, pp. 1227–1235.

[24] Furukawa, J., Hirano, T., and Williams, F. A., 1998. "Burning velocities of flamelets in a turbulent premixed flame". *Combustion and Flame,* ***113***, pp. 487–491.

[25] Ikeda, Y., Kojima, J., Nakajima, T., Akamatsu, F., and Katsuki, M., 2000. "Measurement of the local flamefront structure of turbulent premixed flames by local chemiluminescence". *Proceedings of the Combustion Institute,* ***28***, pp. 343–350.

[26] Furukawa, J., and Williams, F. A., 2003. "Flamelet effects on local flow in turbulent premixed bunsen flames". *Combustion Science and Technology,* ***175***, pp. 1835–1858.

[27] Savarianandam, V. R., and Lawn, C. J., 2006. "Burning velocity of premixed turbulent flames in the weakly wrinkled regime". *Combustion and Flame,* ***146***, pp. 1–18.

[28] Driscoll, J. F., 2008. "Turbulent premixed combustion: Flamelet structure and its effect on turbulent burning velocities". *Progress in Energy and Combustion Science,* ***34***, pp. 91–134.

[29] Kostiuk, L., Bray, K., and Cheng, R., 1993. "Experimental study of premixed turbulent combustion in opposed streams: Part II–Reacting flow field and extinction". *Combustion and Flame,* ***92***, pp. 396–409.

[30] Mastorakos, E., Taylor, A., and Whitelaw, J., 1995. "Extinction of turbulent counterflow flames with reactants diluted by hot products extinction of turbulent counterflow flames with reactants diluted by hot products". *Combustion and Flame,* ***102***, pp. 101–114.

[31] Kostiuk, L., Shepherd, I., and Bray, K., 1999. "Experimental study of premixed turbulent combustion in opposed streams: Part III–Spatial structure of flames". *Combustion and Flame,* ***118***, pp. 129–139.

[32] Geyer, D., Kempf, A., Dreizler, A., and Janicka, J., 2005. "Turbulent opposed-jet flames: a critical benchmark experiment for combustion LES". *Combustion and Flame,* ***143***, pp. 524–548.

[33] Böhm, B., Geyer, D., Dreizler, A., Venkatensan, K., Laurendeau, N., and Renfro, M., 2007. "Simultaneous PIV/PTV/OH PLIF imaging: Conditional flow field statistics in partially premixed turbulent opposed jet flames". *Proceedings of the Combustion Institute,* ***31***, pp. 709–717.

[34] Venkatesan, K., King, G., Laurendeau, N., Renfro, M., and Böhm, B., 2009. "Spatial and temporal characteristics of OH in turbulent opposed-jet double flames". *Flow Turbulence and Combustion,* ***83***, pp. 131–152.

[35] Coppola, G., and Gomez, A., 2009. "Experimental investigation on a turbulence generation system with high-blockage plates". *Experimental Thermal and Fluid Science,* ***33***, pp. 1037–1048.

[36] Coppola, G., Coriton, B., and Gomez, A., 2010. "Experimental study of highly turbulent isothermal opposed-jet flows". *Physics of Fluids,* ***22***, p. 105101.

[37] Coppola, G., Coriton, B., and Gomez, A., 2009. "Highly turbulent counterflow flames: A laboratory scale benchmark for practical systems". *Combustion and Flame,* ***156***, pp. 1834–1843.

[38] Lavoie, P., Avallone, G., De Gregorio, F., Romano, G., and Antonia, R., 2007. "Spatial resolution of PIV for the measurement of turbulence". *Experiments in Fluids,* ***43***, pp. 39–51.

[39] Benedict, L., and Gould, R., 1996. "Towards better uncertainty estimates for turbulence statistics". *Experiments in Fluids,* ***22***, pp. 129–136.

[40] O'Neill, P., Nicolaides, D., Honnery, D., and Soria, J., 2004. "Autocorrelation functions and the determination of integral length with reference to experimental and numerical data". *15th Australian Fluid Mechanics Conference, Sydney, Australia*, December, pp. 1–4.

[41] Yuen, F., and Gülder, O., 2009. "Investigation of dynamics of lean turbulent premixed flames by Rayleigh imaging". *AIAA J.,* ***47***, pp. 2964–2973.

[42] Sutton, J., and Driscoll, J., 2004. "Rayleigh scattering cross sections of combustion species at 266, 355, and 532 nm for thermometry applications". *Optics Letters,* ***29***, pp. 2620–2622.

[43] Knaus, D., Sattler, S., and Gouldin, F., 2005. "Three-dimensional temperature gradients in premixed turbulent flamelets via crossed-plane Rayleigh imaging". *Combustion and Flame,* ***141***, pp. 253–270.

[44] Miles, R., Lempert, W., and Forkey, J., 2001. "Laser Rayleigh scattering". *Measurement Science and Technology,* ***12***, pp. R33–R51.

[45] Pavlidis, T., 1982. *Algorithms for Graphics and Image Processing*. Springer, Berlin, Germany.

[46] Bergthorson, J., Salusbury, S., and Dimotakis, P., 2011. "Experiments and modelling of premixed laminar stagnation flame hydrodynamics". *Journal of Fluid Mechanics,* ***681***, pp. 340–369.

[47] Damkohler, G., 1940. "The effect of turbulence on the combustion rate in gas compounds". *Z. Elektrochem. Angew. Phys. Chem,* ***46***, pp. 601–626.

[48] Sung, C., Law, C., and L Axelbaum, R., 1994. "Thermophoretic effects on seeding particles in LDV measurements of flames". *Combustion science and technology,* ***99***(1-3), pp. 119–132.

[49] Egolfopoulos, F. N., and Campbell, C. S., 1999. "Dynamics and structure of dusty reacting flows: inert particles in strained, laminar, premixed flames". *Combustion and flame,* ***117***(1), pp. 206–226.

[50] Bergthorson, J., and Dimotakis, P., 2006. "Particle velocimetry in high-gradient/high-curvature flows". *Experiments in Fluids,* ***41***(2), pp. 255–263.

[51] Allen, M. D., and Raabe, O. G., 1985. "Slip correction measurements of spherical solid aerosol particles in an improved millikan apparatus". *Aerosol Science and Technology,* ***4***(3), pp. 269–286.

[52] Talbot, L., 1981. "Thermophoresis-a review". *Progress in Astronautics and Aeronautics,* ***74***, pp. 467–488.

[53] Vincenti, W., and Kruger, C., 1965. "Introduction to physical gas dynamics john wiley and sons". *Inc., New York*, pp. 267–268.

APPENDIX

Uncertainty in particle image velocimetry

In Particle Image Velocimetry, PIV, the flow is seeded with tracer particles and the spatial displacement of a particle over a fixed time interval is measured. In PIV, it is assumed that the particle velocity is equal to the fluid velocity, however, this assumption may introduce some uncertainty in the flow velocity measurement due to particle-inertia, thermophoretic, and other

effects. The equation of motion for a particle in a one dimension flow can be expressed using Newtons second law as:

$$\sum F = m_P\, a_P = m_P \frac{\mathrm{d}u_P}{\mathrm{d}t} \tag{7}$$

where $\sum F$ is the sum of the forces acting on the particle, m_P is the mass of a spherical particle, a_P is the particle acceleration, and u_P is the particle velocity. The most important forces that act on a particle in a typical flow are the pressure-gradient force, the fluid-inertial force, the unsteady-drag force, the gravitational force, the Stokes-drag force, and the thermophoretic force. The most commonly used seeding particles in PIV technique, are atomized oil droplets and alumina (Al_2O_3) particles, where the particle density is typically much larger than the fluid density, hence, force terms containing the gas density (pressure-gradient, apparent-mass, and unsteady-drag) are frequently neglected [48]. Furthermore, in these experiments, the gravitational force is also neglected, as it has been shown to have small effect for micron-sized alumina particles [49]. Therefore, in turbulent PIV, the principal sources of uncertainty have reduced to particle lag due to Stokes-drag force (F_{SD}) and thermophoresis (F_{TP}) [50], with small contributions from camera and laser sheet perpendicularity, calibration, and processing algorithm.

In these turbulent experiments, measurement of small scale fluctuations, u', and instantaneous reference flamelet speeds, $S_{u,ref}$, by PIV is of central interest. $S_{u,ref}$ is the velocity prior to the high temperature gradients, therefore, thermophoretic force can also be neglected in analyzing the uncertainty of $S_{u,ref}$. Therefore, the resulting equation of motion for the particle is left with the drag force exerted on a particle. Considering the Stokes drag force in low Reynolds number flow, one can derive the ratio of particle velocity, u_P, to fluid velocity, u_f:

$$\frac{u_P}{u_f} = \frac{1}{1 + C_{KW}\,\tau_s\,\sigma} \tag{8}$$

The details of these calculations and the various terms can be found in [48–53]. In this equation, C_{KW} is the Knudsen-Weber slip-correction factor [51–53], τ_s is the relaxation time or stokes time, and σ is the fluid velocity gradient. In these experiments, the integral length scale, L, and turbulence intensity, u', are the relevant length scale and characteristic velocity scale, respectively:

$$\sigma = \frac{\mathrm{d}u_f}{\mathrm{d}x} = \frac{2\,u'}{L} \tag{9}$$

The stokes time, τ_s, can be derived as:

$$\tau_s = \frac{\rho_P\, \mathrm{d}_P^2}{18\mu} \tag{10}$$

TABLE 3. Uncertainty details of turbulent flames of methane-air at $\phi = 0.6$ ($S_L^o = 11.5$ cm/s), propane-air at $\phi = 0.7$ ($S_L^o = 19.7$ cm/s), and hydrogen-air at $\phi = 0.19$ ($S_L^o = 8.75$ cm/s)

	U[m/s]	u'[m/s]	τ_s[μs]	σ[1/s]	C_{KW}	Uncer.[%]
CH_4	0.5	0.12	12	95.2	1.15	0.13
	0.6	0.17	12	130.3	1.15	0.18
	0.7	0.27	12	214.3	1.15	0.30
	1.1	0.53	12	420.6	1.15	0.58
C_3H_8	0.5	0.2	12	166.6	1.14	0.23
	0.81	0.32	12	269.3	1.14	0.38
	1	0.57	12	470.0	1.14	0.65
	1.4	0.75	12	618.4	1.14	0.86
H_2	0.6	0.14	12	107.3	1.16	0.15
	0.7	0.22	12	164.9	1.16	0.23
	0.9	0.36	12	269.9	1.16	0.37
	1.3	0.92	12	689.7	1.16	0.94

where μ is the fluid viscosity, d_P is the particle diameter, and ρ_P is the particle density .

Experimental conditions and uncertainty details for turbulent combustion experiments are listed in Table 3. As listed in this table, characteristic particle response time in these experiments is: $\tau_s = 12\ \mu s$, resulting in an uncertainty of less than 1% in a high-turbulence intensity case.